Resolution enhancement with improved range Doppler algorithm in high numerical aperture OCT

Xiaodong Chen (陈晓冬)[1,2*], Yong Lei (雷 湧)[1,2], Yi Wang (汪 毅)[1,2], and Daoyin Yu (郁道银)[1,2]

[1] *College of Precision Instrument and Opto-Electronic Engineering, Tianjin University, Tianjin 300072, China*

[2] *Opto-Electronic Information Science and Technical Lab, Ministry of Education, Tianjin University, Tianjin 300072, China*

[*] *Corresponding author: xdchen@tju.edu.cn*

Received June 22, 2011; accepted September 15, 2011; posted online October 31, 2011

The improved range Doppler algorithm is proposed to abate the trade-off between resolutions and depth of focus in spectral domain optical coherence tomography. By considering the finite beam width and the shape of the wavefronts produced by the Gaussian beam, a physical diffraction model is presented to simulate the light propagation process in the sample. The two-dimensional processing of the spectrum data is decomposed into two one-dimensional processings of Stolt transform and matched filter. Experimental results show that image reconstruction can be achieved. The transverse and axial resolutions are both improved significantly, especially in the out-of-focus range, and the resolutions are almost equivalent throughout the entire region of interest.

OCIS codes: 100.3010, 100.2000, 100.2980.

doi: 10.3788/COL201109.121001.

Optical coherence tomography (OCT) is a cross-sectional optical imaging technique with high resolution of 1–15 μm. Since its invention, it has been used in diverse areas of medical imaging[1]. In standard time-domain OCT (TDOCT), special hardware designs for the scanning of the reference are needed, which complicates the instrument and reduces the imaging speed. Spectral domain OCT (SDOCT) measures depth-resolved reflectance of tissues by resampling and Fourier transforming the spectrum data. SDOCT has attracted considerable attention due to its high sensitivity and imaging speed.

In the traditional reconstruction, the resolution in the axial direction and the transverse resolution are determined by the bandwidth of the light source and the numerical aperture (NA), respectively. However, the spot diameter becomes large, and the curvature of wavefronts become significant as NA increases; thus, the transverse and axial resolutions are both related to NA during scanning. Only scatterers in the depth of focus (DOF) range exhibit high resolution and those in the out-of-focus (OOF) range are seriously blurred in both transverse and axial directions. Several methods have been introduced to improve transverse resolution, such as dispersion compensation[2] and wavenumber domain algorithms[3], whereas the light source with non-Gaussian spectral shape has been introduced to improve axial resolution[4]. However, most of these methods are one-dimensional (1D), making them limited. Others have taken account of the phase information of the OCT image and extended for two-dimensional (2D) studies[5,6]; however, the curvature produced by the wavefronts of the light source and transverse scan have not been taken into account.

In this letter, we propose a novel modality that achieves depth-independent resolution, wherein the focus is fixed at one depth and alleviates the compromise between resolutions and DOF in OCT. A 2D scalar diffraction model is derived, and the inverse scattering problem is solved. The matched filter is applied to correct image curvature and axial range cell migration (RCM). In addition, Stolt transform is used to realize the focusing in transverse direction. The numerical diffraction algorithm is similar to the range Doppler algorithm (RDA) of synthetic aperture radar (SAR)[7]. A few limitations of this method employed in the improved RDA, along with some possible extensions of this method, are also discussed.

The OCT system is based on a fiber Michelson interferometer, as illustrated in Fig. 1. The beam from a superluminescent-diode (SLD) source is focused onto a sample while it is scanned transversely over the sample. The probe beam contains components propagating in different directions, as shown in Fig. 2. As the beam is translated over the imaging regions (from the dashed line profile of probe beam to the solid line one), different parts of the probe beam become incident on the scatterer. Therefore, it can be interpreted that a single detection receives contributions from multiple scatterers, and different detections contain contributions of multiple directions from the same scatterer as the probe beam is translating over the sample. Fortunately, the principle of synthetic aperture also meets the physical model of diffraction[8]. Hence, the scalar diffraction

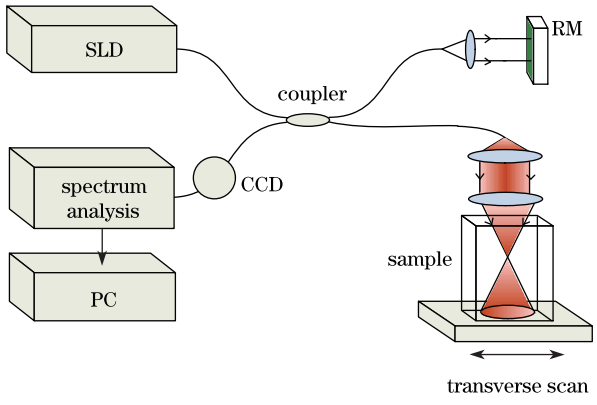

Fig. 1. Schematic of the SDOCT system. RM is reference mirror, PC is personal computer, and CCD is charge-coupled device.

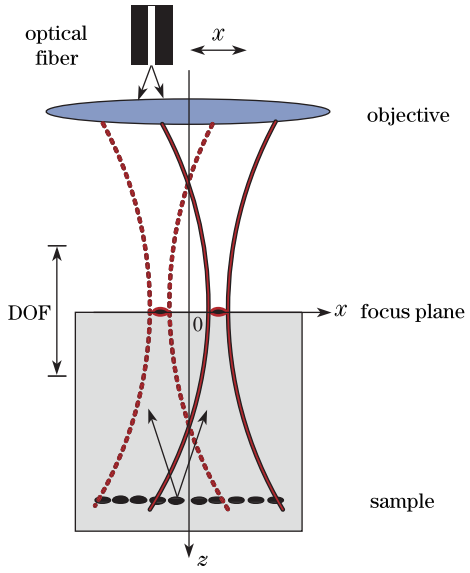

Fig. 2. Illumination in the OCT. The Gaussian beam illuminates a sample.

model can be used to simulate the light propagation process for ballistic and quasi-ballistic backscattered photons.

In the DOF, the beam width is narrow and the scatterers are illuminated for a short interval as the beam is translated transversely, thus allowing them to exhibit high resolution. As the scatterers are away from the focus, the width of the probe beam becomes wide and the scattering signal is returned for a much larger interval. Thus, the point-like scatterers become blurred due to the RCM effect. The method proposed below uses diverse illumination directions to reconstruct the image and correct the RCM effect.

In addition, the curves can be used to represent the constant-time wavefronts of the beam, as illustrated in Fig. 3. As the beam is scanned, the diversity of illumination directions occurs simultaneously with the phase of the wavefronts. This means that the scattered signals have different phases because the scatterer is illuminated by the different parts of the probe beam along the x direction. This can be explained by the Gaussian beam propagating along the z direction as expressed by

$$E(x,z) = E_0 \frac{1}{2\pi\omega^2(z)} \mathrm{e}^{-x^2/[2\omega^2(z)]} \cdot \exp\left\{-\mathrm{i}k\left[z+\frac{x^2}{2R(z)}\right] - \arctan\left(\frac{z}{f}\right)\right\}, \quad (1)$$

where $\omega(z)$ is the spot radius, $R(z)$ is the radius of the equiphase surface, and f is the confocal parameter. In addition, $k\frac{x^2}{2R(z)}$ describes the phase shift related to the transverse coordinate x, which generates the image curvature.

The electric field distribution of the Gaussian beam on the reference mirror and the sample is expressed as

$$E_0(x,\, z;\, k) = A(k) \cdot g(x,\, z;\, k), \quad (2)$$

where g describes the normalized Gaussian beam profile, and $A(k)$ is the power spectral density of the source. The normalized beam profile is given by $g(x,\, z;\, k) = \omega^{-2}(z)\mathrm{e}^{-x^2/2\omega^2(z)}/2\pi$, where $\omega(z) = \omega_0\sqrt{1+(z/f)^2}$, $\omega_0 = \alpha/k$, and $\alpha = \pi/\mathrm{NA}$. In general, the Gaussian beam is focused on the surface of the reference mirror, whose reflectivity is nearly 100%. Thus, the reference field can be written as

$$E_\mathrm{r}(x,\, z;\, k) \approx E_0(x,\, 0;\, k)\exp(-\mathrm{i}k\delta_1), \quad (3)$$

where δ_1 is the phase of the reference field.

The scattered field of a scatterer is composed of different contributions as the probe beam is scanning across the sample, that is, it is an integral over the x and z directions. Thus, the scattered field can be calculated from 2D integral as

$$\begin{aligned} E_\mathrm{s}(x,\, z;\, k) &= \int E'_\mathrm{s}(x,\, z;\, k)G(x,\, z;\, k)\mathrm{d}x \\ &= \iint E_0(x,\, z;\, k)\cdot\eta(x,\, z)\cdot\exp(-\mathrm{i}k\delta_2) \\ &\quad \cdot G(x,\, z;\, k)\mathrm{d}x\mathrm{d}z, \end{aligned} \quad (4)$$

where η is the scattering potential, δ_2 is the phase of scattered field, and G is a Green function $G(x,\, z;\, k) = \mathrm{e}^{\mathrm{i}kr}/r$, where $r = \sqrt{x^2+z^2}$.

According to the principle of interference, the detected intensity $I(x,k)$ is given as

$$\begin{aligned} I(x,\, k) &= [E_\mathrm{r}(x,\, z;\, k)]^2 + [E_\mathrm{s}(x,\, z;\, k)]^2 \\ &\quad + 2E_\mathrm{r}(x,\, z;\, k)E_\mathrm{s}(x,\, z;\, k)\exp(-\mathrm{i}k\delta). \end{aligned} \quad (5)$$

Assuming the autocorrelation terms are negligible, measurements of $I(x,\, k)$ allow the cross-correlation $S(x,\, k)$ to be inferred as

$$\begin{aligned} S(x,\, k) &= E_\mathrm{r}(x,\, z;\, k)E_\mathrm{s}(x,\, z;\, k)\exp(-\mathrm{i}k\delta) \\ &= \iint E_\mathrm{r}(x,\, z;\, k)E_\mathrm{s}(x,\, z;\, k)\exp(-\mathrm{i}k\delta)\mathrm{d}x\mathrm{d}z, \end{aligned} \quad (6)$$

where the phase difference δ between the reference and scattered fields is given by $\delta = kn\frac{x^2}{2R(z)} + 2knr$, where n is the refractive index of the sample.

Taking the transverse spatial Fourier transform of $S(x,\, k)$, we obtain $\widetilde{S}(k_x,\, k)$ and the 2D Fourier transform of the sample is $\widetilde{\widetilde{S}}(k_x,\, k_z)$. This is the result of

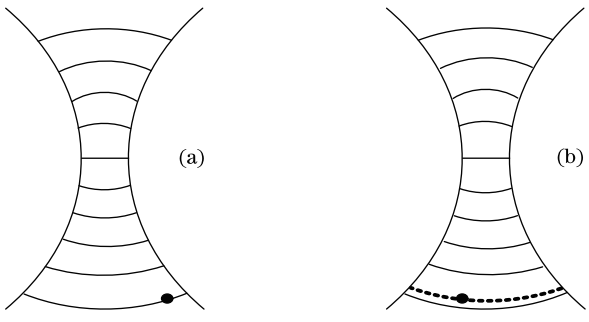

Fig. 3. Illustration of how the image curvature is generated. Parts (a) and (b) different wavefronts providing phase diversity in the scattered signal.

the scattering from different detections during transverse scanning, which then leads to RCM. Our previous research has corrected RCM in transverse direction with Stolt transform[5]. In order to achieve focusing, Stolt mapping $k_z = \sqrt{k^2 - k_x^2}$ warps the coordinate space to $\widetilde{S}(k_x, k_z)$, which removes the signals to zero Doppler position, as shown in Fig. 4. The dashed lines show the wavefronts of the probe beam (AD is the distance between them). The distances of AB and AC are represented by λ_x and λ_z respectively, which also introduce the spatial wavenumbers of k_x and k_z. Then Stolt interpolation is needed to resample the result back to a regular grid to facilitate numerical processing.

The corrections of axial RCM and curvature can be realized with matched filter, a method that has been used in the Fourier reconstruction methods of SAR. The simplest matched filter is the conjugation of the phase difference δ, and its expression can be written as

$$H(x, z; k) = \exp\left\{\mathrm{j}kn\left[\frac{x^2}{2R(z)}\right]\right\} \cdot \exp[\mathrm{j}2kn(r - z)]. \quad (7)$$

Here $H_1(x, z; k) = \exp\left\{\mathrm{j}kn[\frac{x^2}{2R(z)}]\right\}$ is used to correct the curvature produced by the wavefronts, and $H_2(x, z; k) = \exp[\mathrm{j}2kn(r - z)]$ is used to eliminate the RCM in the axial direction. With the help of the filter, axial compression is achieved effectively and resolution is improved greatly.

Figure 5 shows the procedure of improved RDA. The result of each image processing is vividly demonstrated in Fig. 5(a), and the procedure is summarized in the flow diagram shown in Fig. 5(b).

On the basis of the theoretical derivation above, the potential of the solution of the inverse scattering problem was explored through numerical simulation. A unit-amplitude point scatterer located on the z axis with axial offset 400 μm was considered for the present work. Here, 2 lens with high NAs (NA = 0.2 and 0.5, respectively) effectively demonstrated the results of the resampling scheme; they also illustrated the possibility of achieving image reconstruction with such high NAs. The 2D data were collected for 400 evenly spaced wavenumbers between 4.42 $\mu\mathrm{m}^{-1}$ (1 420 nm wavelength in free space) and 5.15 $\mu\mathrm{m}^{-1}$ (1 220 nm).

In Fig. 6, the results of the simulated imaging of this object are shown. In the case of standard OCT reconstructions, the simulation results start to deviate

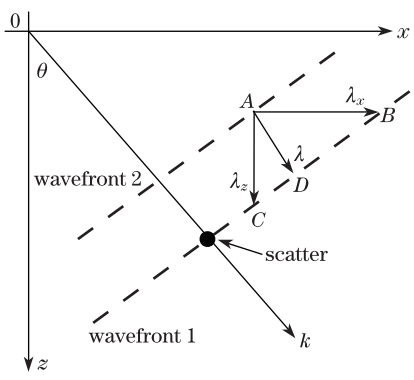

Fig. 4. Schematic of Stolt mapping.

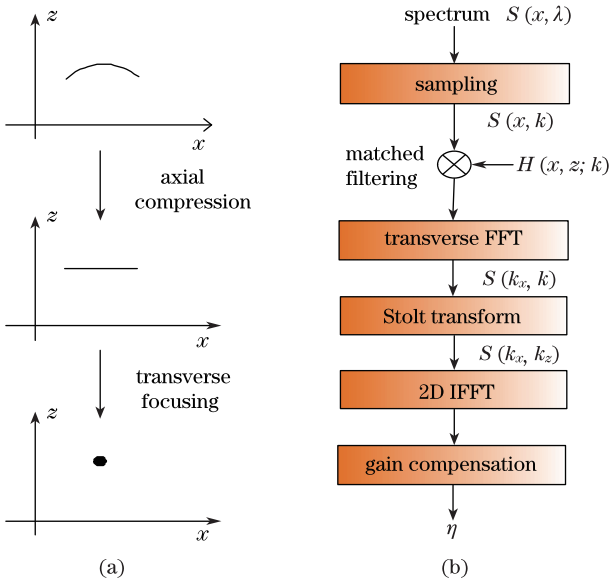

Fig. 5. Procedure of improved RDA: (a) schematic of image processing and (b) flow diagram of the method.

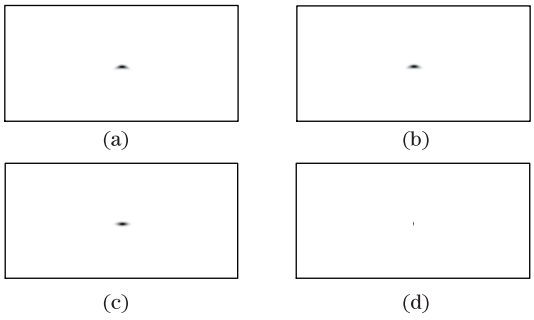

Fig. 6. Reconstruction images of single scatterer on NA = 0.2. (a) Unprocessed data, (b) correction of curvature, (c) correction of curvature and RCM in the axial direction, and (d) improved RDA.

as they move away from the focus, as shown in Fig. 6(a). Compared with traditional OCT reconstruction, the matched filter not only corrects the curvature produced by wavefronts of Gaussian probe beam (Fig. 6(b)), it also eliminates the RCM in the axial direction (Fig. 6(c)). Thus, a curved image is corrected to be a transverse line and the axial data is compressed. When the transverse focusing is implemented by Stolt transform, the scatterer becomes more pointlike (Fig. 6(d)). The proposed method does an excellent job of restoring the OOF scatterer. The axial resolution is improved from 2.5 to 1 μm. The images in Fig. 7 are the simulation results of the single scatterer with a lens whose NA is 0.5. It illustrates that the improved RDA is also applicable for higher NAs.

In order to demonstrate the influence of the finite beam width, two scatterers at different depths were considered, as shown in Fig. 8. As depths become bigger, the beam widths become wider too, making the curvature of images more obvious (Fig. 8(a)). With the improved RDA, two point-like images can be achieved (Fig. 8(b)), indicating that the resolutions are improved significantly. However, since the spectrum of light source has not been considered, the reconstruction of a point-like scatterer is

a short line rather than an ideal point.

To experimentally validate this method, we established the SDOCT system. Light from a SLD ($\lambda = 1\,310$ nm, $\Delta\lambda = 200$ nm) was divided by a 50/50 fibre-optic coupler (splitter) between a reference arm and a sample arm. The focal length of the objective was 10 mm and NA was 0.2, which set the DOF at 20.86 μm. An interferometer with a 512-element charge-coupled device (CCD) was used to detect the interference spectrum of the scattered light from the sample and the reflected light reflected by reference mirror.

We used fresh pig liver as the sample in our experiment. The probe beam was focused on the top of the liver so that the defocus and blurring appeared on the underside of the surface of the tissues. Scatterers are poorly resolved in the image (Fig. 9(a)), and become sharp and distinct after the improved RDA processing (Fig. 9(b)). Resolution improvements can be seen across the liver tissue, where cell boundaries are obscured by the RCM effect in the OCT image, but are made clear in the improved RDA image. Moreover, the SNR improved from to 65 to 80 dB. The transverse and axial resolutions also improved significantly, especially in the OOF range. In addition, the resolutions are almost equivalent through the entire region of interest, as shown in the dashed retangles.

The improved RDA obviates the trade-off between DOF and resolutions, and enables the use of much higher NA optics without loss of depth of imaging. With the proposed method, the nearly indistinct and featureless planes in the traditional OCT come to be the meaningful ones that may have potential diagnostic value. In addition, the improved RDA makes it possible to carry out micrometer-scale *vivo* imaging rather than resecting these tissues. The fringe artifacts in

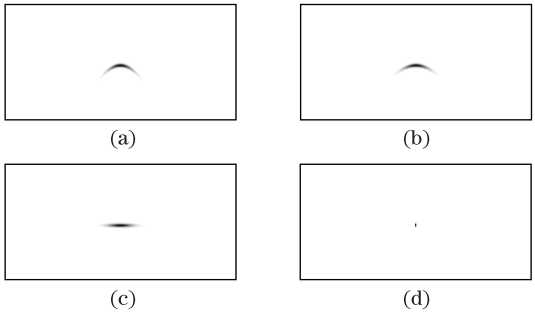

Fig. 7. Reconstruction images of single scatterer on NA = 0.5. (a) Unprocessed data, (b) correction of curvature, (c) correction of curvature and RCM in the axial direction, and (d) improved RDA.

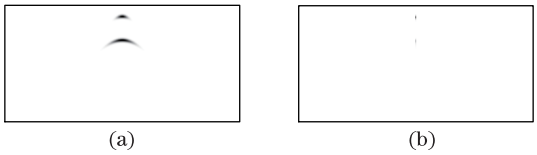

Fig. 8. Reconstruction images of two scatterers on NA = 0.5. (a) Unprocessed data and (b) improved RDA.

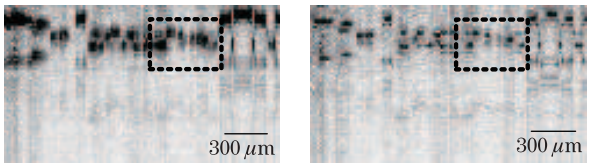

Fig. 9. An image of fresh pig liver (a) without and (b) with improved RDA.

the images are probably due to the multiple scattering or interference between adjacent scatterers. The increased resolution gained by the solution to the inverse scattering problem relies upon the phase stable measurements, whereas the scanning fluctuations affect the phase stability. Further research might account for nonlinear scanning attributable to sample or probe motions, vignetting, and aberrations due to the finite pupil of any realistic optical instrument in the forward model, and so on. Future research must focus on developing OCT signal processing algorithms in order to increase processing speed, accounting for heterogeneities of refraction index in the tissues.

In conclusion, using a 2D scalar diffraction model, we derive and demonstrate an improved RDA to cancel the defocusing effect observed in OCT images. The improved transverse resolution is achieved by Stolt transform, whereas axial resolution is achieved by matched filter. Experimental results have shown that, compared with the standard OCT methods, the proposed method can realize significantly better image reconstruction with spatially invariant resolution through the entire region of interest. This result demonstrates the promising capability of the proposed model. Although the matched filter is used in OCT, it can also be applied to the correction of coherence gate curvature in optical coherence microscopy.

This work was supported by the National Natural Science Foundation of China under Grant No. 30800245.

References

1. G. Moneron, A. C. Boccara, and A. Dubois, Opt. Lett. **30,** 1351 (2005).
2. D. L. Marks, A. L. Oldenburg, J. J. Reynolds, and S. A. Boppart, App. Opt. **42,** 204 (2003).
3. X. Chen, Q. Li, Y. Lei, Y. Wang, and D. Yu, Opt. Comm. **283,** 1993 (2010).
4. I. Hsu, C. Sun, C. Lu, C. Yang, C. Chiang, and C. Lin, App. Opt. **42,** 227 (2003).
5. P. D. Woolliams, R. A. Ferguson, C. Hart, A. Grimwood, and P. H. Tomlins, App. Opt. **49,** 2014 (2010).
6. T. S. Ralston, D. L. Marks, P. S. Carney, and S. A. Boppart, Nat. Phys. **3,** 129 (2007).
7. I. G. Cumming and F. H. Wong, *Digital Processing of Synthetic Aperture Radar Data*: *Algorithms and Implementation* (Artech House, Massachusetts, 2004).
8. L. Yu, B. Rao, J. Zhang, J. Su, Q. Wang, S. Guo, and Z. Chen, Opt. Express **15,** 7634 (2007).